Available online at www.sciencedirect.com
ScienceDirect
Journal of Sound and Vibration 323 (2009) 877–895
JOURNAL OF SOUND AND VIBRATION
www.elsevier.com/locate/jsvi

Mass loaded resonance of a single unit impact damper caused by impacts and the resulting kinetic energy influx

Jongchan Park[a], Semyung Wang[a,*], Malcolm J. Crocker[b]

[a]*Department of Mechatronics, Gwangju Institute of Science and Technology, 1 Oryong-dong, Buk-gu, Gwangju 500-712, Republic of Korea*
[b]*Department of Mechanical Engineering, Auburn University, Auburn, AL 36849, USA*

Received 22 October 2008; accepted 8 January 2009
Handling Editor: L.G. Tham
Available online 25 February 2009

Abstract

This paper presents experimental and numerical investigations of resonance vibrations of an impact damper other than at its original resonance frequency. In the numerical modelling of impacts, the principle of conservation of momentum is employed. An improved scheme is proposed for identifying the time of contact and calculation of the state variables after impact. This scheme avoids false detection of collisions and embodies collisions or contacts with infinitesimally small differences in velocities. Descriptions of the motion trajectories and how the relative phase of the impact contributes to the momentum transfer and degree of damping are presented. Numerical simulations are in good agreement with experimental results with respect to the general performance and the shift in resonance which occurs with large amplitude excitation. The novel feature of this paper is the modelling of the mass loading effect of impacts through the transfer of kinetic energy.
© 2009 Elsevier Ltd. All rights reserved.

1. Introduction

Noise and vibration are of concern with many mechanical systems including industrial machines, home appliances, transportation vehicles, and building structures [1]. Many such structures are comprised of beam and plate like elements. The vibration of beam and plate systems can be reduced by the use of passive damping, once the system parameters have been identified [1–5]. In some cases of forced vibration, the passive damping that can be provided is insufficient and the use of active damping has become attractive. The rapid development of micro-processors and control algorithms has made the use of active control feasible in many practical situations [6–8]. The field of active control is now of considerable interest to researchers, for example in ships, rotating systems, industrial machinery and flexible structures.

Vibration control using passive damping is often preferred in most practical applications due to its low cost. One such passive damping approach utilizes momentum transfer between a primary system and auxiliary

*Corresponding author. Tel.: +82 62 970 2390; fax: +82 62 970 2384.
E-mail address: smwang@gist.ac.kr (S. Wang).

0022-460X/$ - see front matter © 2009 Elsevier Ltd. All rights reserved.
doi:10.1016/j.jsv.2009.01.044

Nomenclature

a'	normalized displacement amplitude of base $a' = X_0\omega_n^2/g$
c	damping constant of the vibratory system
d	clearance of auxiliary mass and primary mass
e	coefficient of restitution of impact
F_0	excitation force on primary system
g	acceleration of gravity
k	stiffness of the vibratory system
m_a	mass of auxiliary mass
m_p	mass of primary mass
r	frequency ratio of driving frequency to natural frequency
TM	transmissibility of input and output displacement: $\mathrm{TM} = X_p/X_0$
X_a	displacement of auxiliary mass
X_p	displacement of primary mass
$\dot{X}_p$	velocity of primary mass
$\dot{X}_p$	velocity of auxiliary mass
X_0	input displacement
$X_{0\mathrm{ref}}$	reference input displacement of frequency sweep
$\dot{X}_{\mathrm{pabs}}$	Fast-Fourier transformed velocity of primary mass
η	ratio of auxiliary mass to primary mass
Λ	normalized kinetic energy transfer
Φ	mass normalized relative momentum transfer
ψ	displacement ratio: $\psi = X_p/d$
ω	circular driving frequency (rad/s)
ω_{in}	circular resonance frequency under periodic impact (rad/s)
ω_n	circular natural frequency (rad/s)

masses during collisions in order to reduce severe vibrations. Impact damping can be divided into two main types: (1) damping caused by particles, and (2) damping caused by auxiliary masses attached to the overall system. Typically, particle impact damping (PID) uses particles to increase damping by the insertion of the particles into an enclosure attached to the primary vibrating structure. These auxiliary particles absorb kinetic energy of the primary system and convert it into heat, or high-frequency sound and structural vibrations through the inelastic collisions between the particles themselves, and with the enclosure [9–11]. By comparison, a single unit impact damper uses an auxiliary mass enclosed within a cavity inside the primary system. The dynamic response and performance of single unit impact dampers has been studied extensively. Pioneering research was conducted by Paget [12]. Further research by Grubin [13] determined the existence of the optimal distances between the primary mass and the auxiliary mass for the impact damper. Masri [14,15] presented a piecewise analytical solution for the dynamics of an impact damper, and determined that the most effective damping condition occurred with two symmetric collisions per cycle. This was subsequently confirmed [16–18]. Ema and Marui [19] reported that, in the decay of free vibration of a spring mass system, the damping rate of the system increases with a corresponding increase in vibration amplitude. They concluded that the best damping performance occurs for particular combinations of the mass and clearance ratios and depends on the initial spring displacement. They further stated that, with a vertical impact damper, the critical amplitude above which the impact damper ceases to function is determined by the impact damper's original natural frequency and the acceleration of gravity. Cheng and Wang [20] modelled the impact system with a spring and viscous damper to investigate the deformation of the impact damper, and demonstrated that the effective reduction of the vibration response depends primarily on the type of collision encountered by the system. Chatterjee and Mallik [21] and Luo et al. [22] studied stability and bifurcation of impact systems.

It is noted that most of the previous investigations were focused on parameter studies of the optimum system response at the original resonance frequency. Few investigators focused on the performance of impact dampers over a wide range of excitation frequencies and response amplitudes. However, of particular note is that Popplewell et al. [17] and Bapat and Sankar [23] reported, in their investigations of forced vibration, that an impact damper produces negative damping at frequencies lower than that of the original natural frequency and that the structure will vibrate more with, than without, the impact damper. Furthermore, Masri and Ibrahim [16] and Duncan et al. [24] reported that the damping, which occurs at very large excitation

amplitudes, approaches the detuned value, which corresponds to the case when the particle masses are moving together with the structure.

Along with determining the optimum reduction in vibration at the original natural frequency, avoiding resonances which are shifted away from the original natural frequency is an important issue from a practical point of view. In this context, the occurrence of vibration at resonance needs to be fully understood with regard to both operational conditions and system parameters; all of which have yet to be presented experimentally and explained.

Osire et al. [25] detected a shift in the resonance of the vibration in their experiments but did not deal with the mechanics of this phenomenon. Nor did they explain when it occurs and how it is related to the system parameters.

Today, global warming and climate change issues [26,27] are of great concern around the world. In an effort to curb ever increasing power consumption and energy costs, improved inverters have been developed, which are beginning to replace conventional systems. It is generally well known in the industry that using an inverter to control the rotation of the motors used in fans, blower, pumps and compressors can save between 30% and 60% of the energy costs compared with conventional motors [28]. Using an inverter control allows the motor to be driven at the required number of revolutions per minute. In this way, it is possible to allow only the required amount of hydraulic power to be generated and transmitted [29–33].

It is essential to avoid exciting a system with a forcing frequency that is the same as its natural frequency; otherwise enormous vibration amplitudes can occur. These can only be controlled by adding passive or active damping to the system. Thus, the main emphasis of this paper is on the resonance characteristics of an impact damper. Even though there have been some investigations [17,23,24] into the dynamic behavior of impact dampers over a wide range of frequencies, the excitation amplitude and mass ratio of the auxiliary mass have normally been restricted so that either a shift in the resonance frequency does not occur, or the shift in the value is so small that the shift is not noticeable.

In this paper, experimental studies and numerical simulations are presented which demonstrate that a shift in the resonance frequency of an impact damper depends on both the excitation amplitude and the auxiliary mass. In fact, unlike the occurrence of resonance in a linear system, resonance in an impact damper has a strong nonlinear dependence on the vibration amplitude.

Along with the experimental data presented, descriptions of the mass motion demonstrate how the relative motion or phase of impacts affects momentum transfer, and highlights the shift in the resonance frequency caused by the impacts through the influx of kinetic energy and the relationship of this shift to the vibration amplitude.

In our numerical model for the impacts, a modified scheme is proposed for detecting collisions or particle contacts. In this method, information about the previous calculation step is used to prevent false prediction of contacts, termed as 'negative collisions' in this paper. So called negative collisions are numerical errors, which are predicted where one object penetrates the other. These errors can be insignificant in some cases for certain solutions of the variables, even if penetration or overlap of the objects occurs. In our research study, however, the errors caused by negative collisions with large amplitude excitation have been found to be significant. Consequently, sustained motion in which the auxiliary mass is propelled by the primary mass and therefore the two masses move together is employed to guarantee that the contact condition of the auxiliary mass is at grazing incidence for large amplitude oscillations.

2. Physical model and experimental set-up

An impact damper system consists of a cart fixed at the middle of a fixed-fixed circular beam, and a freely moving mass located between the two columns of the cart. The cart is limited strictly to motion in the x-direction on the $x–y$ plane by a low-friction linear guide. Excitation is imparted to the cart by a shaker through a circular beam. The primary difference between our experimental set-up and those used in previous studies [9,20,35,36] is that the system is driven with a prescribed motion, not by a force input. A schematic diagram of the current experimental set-up and measurement equipment is given in Fig. 1.

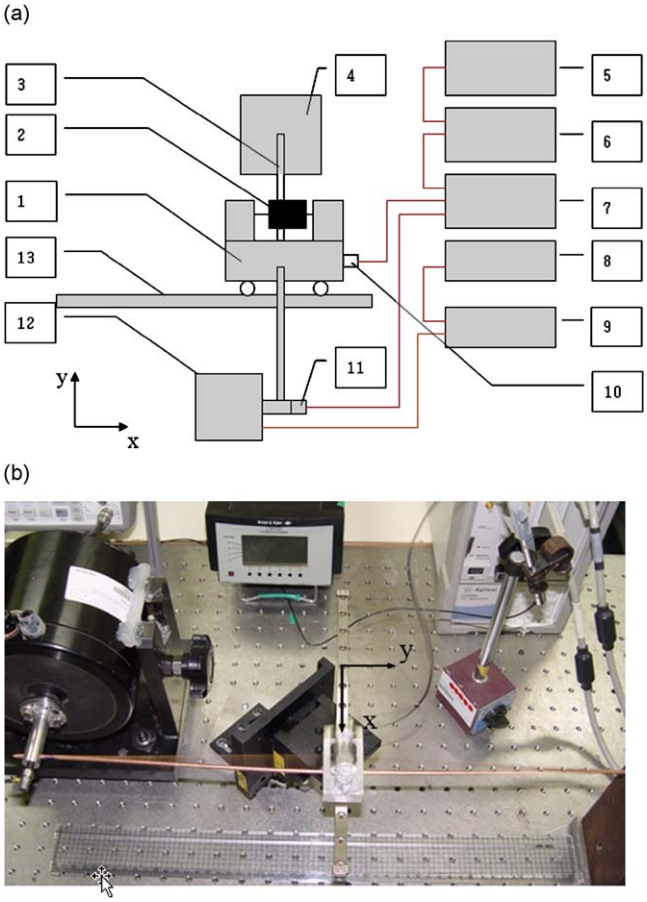

Fig. 1. Experimental set-up. (a) schematic diagram: 1, moving cart; 2, auxiliary mass; 3, fixed–fixed circular beam; 4, rigid block; 5, personal computer; 6, signal analyzer; 7, signal conditioner; 8, function generator; 9, power amplifier; 10, accelerometer (output); 11, accelerometer (input); 12, electromagnetic shaker; and 13, low-friction linear guide; (b) photograph of the system in oscillating motion.

Table 1
Specifications of the primary system and the auxiliary mass.

Items	Mass (gram)	Length (mm)
Pipe (moving part)	18.2	485
Cart (aluminium)	73	
Auxiliary mass (steel)		
$d = 2.6$ mm	45.9	
$d = 4.0$ mm	32.1	

As can be seen, rigid clamping of the beam to the shaker makes it possible to impart a motion to the cart, instead of a force. For the given system, force excitation with a soft spring is inadequate to impart a wide range of excitation amplitudes to the cart, a method conventionally used for the impartation of the excitation force. Therefore, the accelerations of the clamping jig and the cart are measured and used to determine the frequency response function or transmissibility (TM) of the system. In the present paper, TM, the ratio of the cart displacement to that of the input, is used to estimate the degree of damping. Further specifications of the system and auxiliary masses are given in Table 1.

3. Numerical modelling of the impact system

3.1. Modelling of the system

For numerical analysis, the impact damper system is modelled using a two-degree of freedom system with an equivalent linear stiffness constant k, effective primary mass m_p, auxiliary mass m_a and viscous damping constant c, as shown in Fig. 2. The corresponding equations of motion can be written as

$$m_p\ddot{X}_p + c\dot{X}_p + kX_p = F_0 \sin(\omega t), \tag{1}$$

$$m_a\ddot{X}_a = 0, \tag{2}$$

where the superscript dots refer to differentiation with respect to time, and the subscripts "a" and "p" represent physical values of the primary and auxiliary masses, respectively.

FEA (finite element analysis) was utilized in order to calculate the equivalent linear stiffness of the beam. In the calculations, the corresponding generalized primary mass was 1 kg, and the generalized stiffness was 22848.9 N/m, and a value of 4.2% was used for the modal damping from the experiment. Also, 40% of the beam mass was added to the primary mass. Fig. 3 compares the frequency response functions (FRF) obtained from the experiment and numerical simulations without the auxiliary mass present. Note that a fourth-order Runge–Kutta method was used for the numerical computations, and fast-Fourier transformed values of the displacement of the primary mass were used to represent the magnitude of the vibration.

Furthermore, in order to determine the correlation between the experiments with prescribed motion inputs and the numerical simulations with prescribed force inputs, the following relation between force and base motion (input displacement) was utilized:

$$F_0 = X_0\sqrt{k^2 - c^2\omega^2}, \tag{3}$$

where X_0 is the magnitude of the input displacement, ω is the driving frequency in radian/s, and F_0 is the magnitude of the driving force.

3.2. Modelling of the impact

It was assumed that the impacts are instantaneous, each with zero duration; then the impacts between the primary mass and auxiliary mass were implemented by updating the state variables with calculated values after the impact at each step in the numerical analysis. On the basis of the conservation of linear momentum, and using the coefficient of restitution e, Eq. (6), the updated state variables [18,23] were calculated from

$$\dot{X}_p^+ = \frac{(1-\eta e)}{(1+\eta)}\dot{X}_p^- + \frac{\eta(1+e)}{(1+\eta)}\dot{X}_a^-, \tag{4}$$

$$\dot{X}_a^+ = \frac{(1+e)}{(1+\eta)}\dot{X}_p^- + \frac{(\eta-e)}{(1+\eta)}\dot{X}_a^-, \tag{5}$$

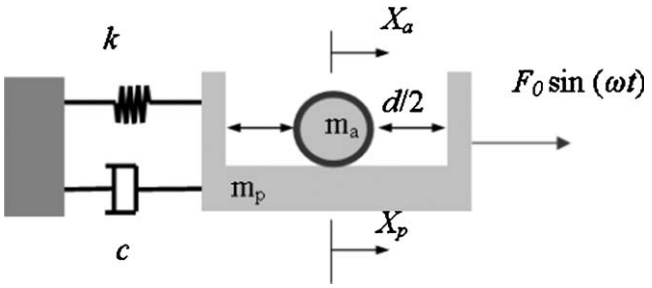

Fig. 2. Two degree of freedom system model used in numerical analysis.

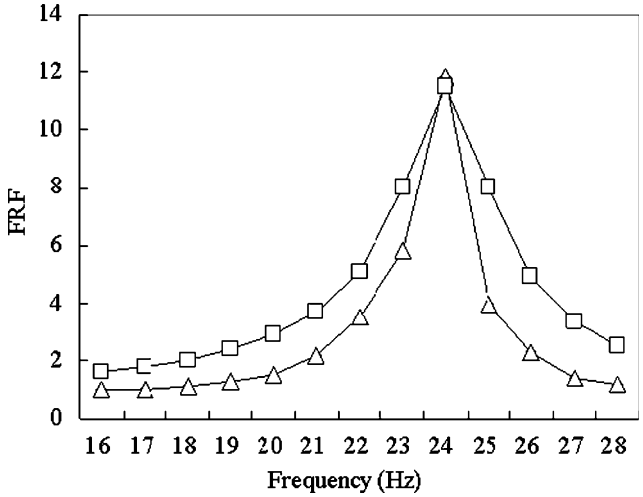

Fig. 3. Numerical and experimental frequency response functions, FRF, of system without auxiliary mass: △—experiment, □—analytical results, $X_{0\mathrm{ref}} = 0.53\,\mathrm{mm}$, $F_0 = 12\,\mathrm{N}$.

$$e = -\frac{(\dot{X}_p^+ - \dot{X}_a^+)}{(\dot{X}_p^- - \dot{X}_a^-)}, \tag{6}$$

where η is the mass ratio m_a/m_p and the superscripts "+" and "−" represent the states just before and after the impact, respectively.

In a numerical study of an impact system, it is imperative to determine the time of occurrence of the collision or impact. To accomplish this, the most frequently used scheme [14,19–23,37] for identifying the time of impact (see Eq. (7)) was utilized to check whether the relative displacement is less than the given criterion value or not. The use of additional iteration algorithms such as bisection [18,38,39] procedures are also sometimes used.

$$R(|X_p(t_{n+1}) - X_a(t_{n+1})|) - d/2 \leqslant R_c, \tag{7}$$

where R refers to the relative location of the masses, d is the clearance, R_c is the criterion value, and the subscript $n+1$ at time t refers to the number of steps in the analysis.

However, the results obtained from the conventional simulation scheme predict that the time of contact is such that the two masses occupy the same physical space, resulting in the impossible situation that the two masses pass through each other without collision. This would occur for a relative position $R_{(t_n)}$ when the time step t_n has a value larger than the criterion R_c so that the impact would occur at time step t_{n+1}. This would predict a so-called "negative collision", as shown in Fig. 4(a).

The error in the detection of collisions caused by a negative collision is negligibly small when the impact and separated motion for each mass dominate the dynamics of the system. Conversely, the error can be too great to ignore if repeated contacts with negligibly small differences in velocities of the primary and auxiliary masses occur. This kind of dynamic behavior is important when the excitation amplitude is large compared to the clearance.

As such, when impacts with infinitesimally small differences in velocities [40,41] of the primary and auxiliary masses occur in the numerical analysis, the relative position remains within the criterion R_c in the following numerical time step. Additionally, this can repeatedly produce "negative collisions" until the auxiliary mass becomes separated from the primary mass. This numerical simulation would produce an unrealistic energy loss in the system due to the fact that a negative collision is impossible in the real world. However, for large mass ratios, errors caused by negative damping are significant in numerical simulations of the system. When the differences in relative velocities and mass values are small, the momentum transfer resulting from particle impacts is also small so that the velocities of both the primary mass and auxiliary mass decrease in proportion to the coefficient of restitution. Decreased velocities of the primary and auxiliary masses make the system stay

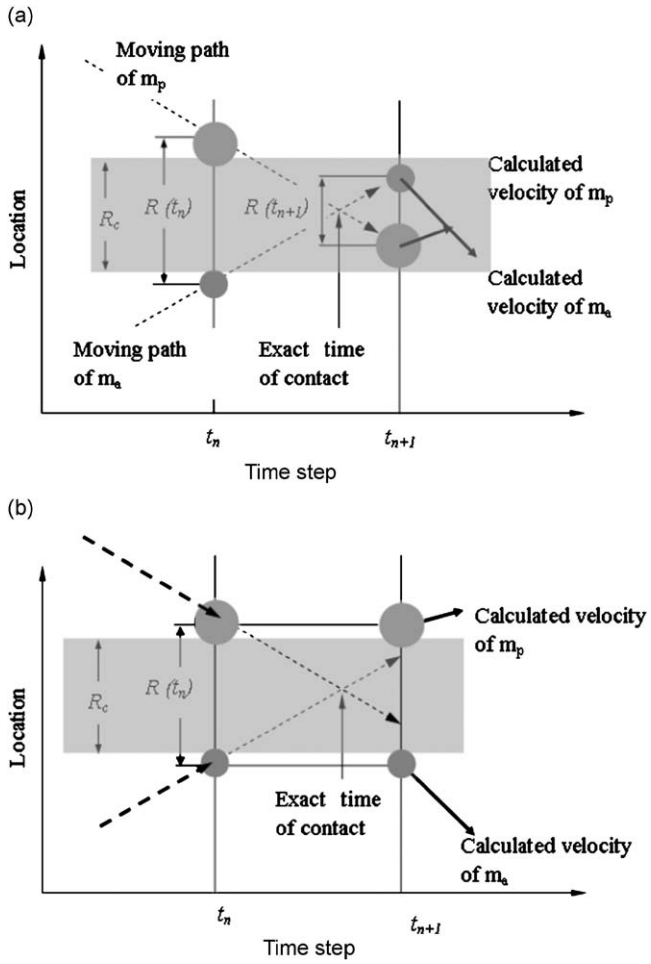

Fig. 4. Numerical simulation, trajectories of primary and auxiliary masses: (a) negative collision; (b) improved scheme: assuming a collision occurs whenever the distances between two masses is less than zero, the state variables after impact are calculated using the state variables at time step t_n.

continuously within the relative difference criterion R_c. In total, the numerical error created by a negative collision has a vibration magnitude less than in the experiments because of the repeated negative collisions caused by large amplitude excitations. Seemingly, this kind of error seems to occur only when the mass changes its direction and the velocity of the primary mass is small. Experiments and numerical simulations carried out in this research show that numerical errors, which represent smaller magnitudes of vibration than in the experiments, can occur even when the system velocity is large for the large excitation amplitudes. In order to overcome these problems in the numerical analysis, an improved scheme for identifying particle contact was developed. In this scheme, impact conditions are confirmed whenever the relative position is less than half of the clearance, as given by Eq. (8).

$$R(|X_p(t_{n+1}) - X_a(t_{n+1})|) - d/2 \leqslant 0. \tag{8}$$

With this condition, it is assumed that a collision occurs after two masses have passed thorough each other. However, state variables after an impact are calculated with state variables at the time step t_n, as given by Eqs. (9) and (10), not at the time step t_{n+1} at which time the two masses have already overlapped.

$$\dot{X}_p(t_{n+1}) = f\langle \dot{X}_p(t_n), \dot{X}_a(t_n) \rangle, \tag{9}$$

$$\dot{X}_p(t_{n+1}) = f\langle \dot{X}_p(t_n), \dot{X}_a(t_n)\rangle, \tag{10}$$

where the brackets $\langle\ \rangle$ denote the calculation of the state variable at impact.

Fig. 4(b) shows the time of collision and the calculation of the state variables. The consequence of this new criterion avoids self-induced repeated collisions; in the case of repeated negative collisions the auxiliary and primary masses are moving together. Hence, sustained motion is more realistic than the occurrence of self-induced repeated collisions or "negative collisions." This is due to the fact that large values of the mass ratio and coefficient of restitution cause a separation velocity much smaller than the approach velocity. This results in continuing collisions being predicted by the conventional method. Furthermore, the error resulting from the relative displacement, R_c, which is the difference between the exact relative distance and distance criterion R_c was eliminated by using trigonometric tracing [42] of the exact time of contact. With these assumptions about the numerical errors as well as the negative collisions, a more precise simulation of the system was carried out. Errors with a large mass ratio value have been reported previously [23]. A comparison between the analytical results obtained with the conventional and proposed methods is given later.

4. Dynamic behavior of the impact damper

The experimental frequency responses shown in Fig. 5 demonstrate a considerable reduction in the measured vibration amplitude of the primary mass, especially around the original resonance frequency of 24 Hz after the installation of an auxiliary mass with the same conditions as given in Fig. 3. The term 'resonance frequency' used throughout this paper refers to the original resonance frequency of the system without attachment of the auxiliary mass, which was 24 Hz.

Fig. 6 further represents the TM of the experiments and the numerical simulation at the original resonance frequency. For the numerical simulation, the value of the coefficient of restitution was set at 0.2. To this extent, TM in Fig. 6 illustrates how the system responds to varying input amplitudes at the original resonance frequency and highlights the fact that no significant change is observed in the experimental values of TM. This further confirms the fact that the frequency responses seen in Fig. 5 are generally representative of the damping characteristics of the impact damper.

Numerical simulations generally predict higher values of TM than those that are measured. The primary reason for the higher values of TM is thought to be a result of neglecting the friction between the primary and auxiliary masses. In a real situation the auxiliary mass cannot move without friction. Despite the discrepancy in magnitudes, the numerical simulation results agree qualitatively with experimental data.

Figs. 5 and 6 demonstrate the usefulness of the impact damper in reducing the displacement of the oscillating structure at the original resonance frequency. But, as stated previously, this research is focused on the resonance characteristics of the impact damper over a wide range of frequencies and excitation amplitudes.

Fig. 7 presents TM values from experiments and numerical simulations for the two test conditions given in Table 2. This figure reveals some intriguing features about the impact damper. Most notable is the fact that the use of the impact damper drastically decreases the displacement of the primary mass at the original resonance

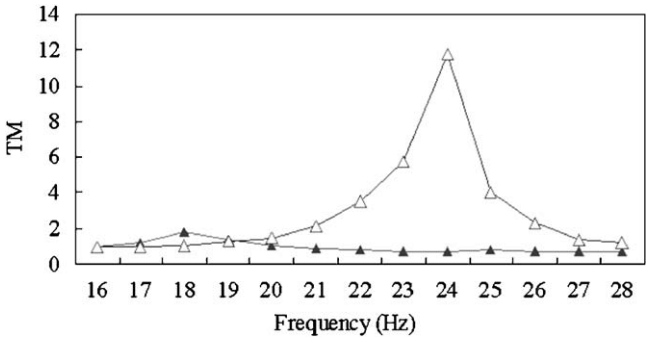

Fig. 5. Experimental frequency responses, TM, of the primary mass: △—without auxiliary mass, ▲—with auxiliary mass ($d = 2.6$ mm, $\eta = 0.57$, $X_{0\text{ref}} = 0.53$ mm).

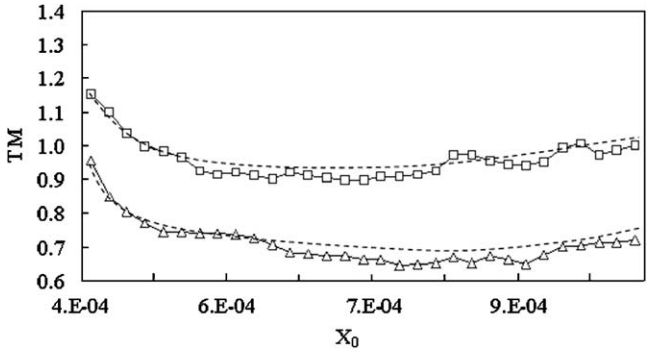

Fig. 6. Transmissibility, TM, as a function of the input displacement: △—experimental results, □—numerical analysis results: broken lines are trend lines of the experimental and numerical results, respectively.

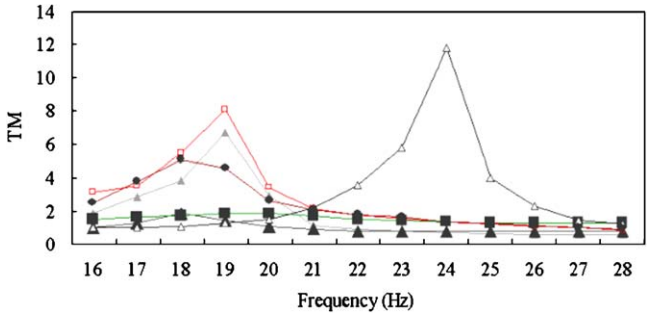

Fig. 7. Numerical and experimental frequency responses: △—experimental results without auxiliary mass with $X_{0\mathrm{ref}} = 0.53$ mm; other conditions listed in Table 2, ▲—Exp_a; ▲—Exp_b; ■—$Numr_a$; □—$Numr_b$. ●—$F_0 = 18$ N.

Table 2
Conditions for the experiments and numerical simulations shown in Fig. 7 ($d = 2.6$ mm, $\eta = 0.57$).

	F_0 (N)	$X_{0\mathrm{ref}}$ (mm)
Exp_a		0.53
Exp_b		0.97
$Numr_a$	12	
$Numr_b$	22	

frequency, and that there is little negative effect of large vibrations or resonance for input cases with small values of Exp_a and $Numr_a$. However, for cases with large input values of Exp_b and $Numr_b$, distinctive resonance peaks are observed, which are shifted to a frequency of 19 Hz.

Experimental results and numerical simulations are shown in Fig. 7. Fig. 8 illustrates the nonlinear behavior of the impact damper as a function of the input amplitude. The TM curves in Fig. 8 were measured experimentally and predicted numerically and are analyzed at 19 Hz. They show two clearly distinguished TM slopes with respect to the input amplitudes. (They are shown as dotted and broken lines.)

It can be seen further in Fig. 8 that the gradient in the right hand half of the curves is approximately five times greater than in the first half of the curves. This transition of TM at 19 Hz, which is related to the increase in input amplitude, has been investigated along with the resonance peaks shown in Fig. 7 with higher experimental input values of Exp_b and $Numr_b$. Hence, in order to study the nonlinear characteristics and their relationship to the input amplitudes more precisely, the time trajectories of the experiments and numerical simulations were conducted. As shown in Fig. 6, damping effects are large over the entire range of input amplitudes when the system is operated at the original resonance frequency. Fig. 7, however, shows a drastic

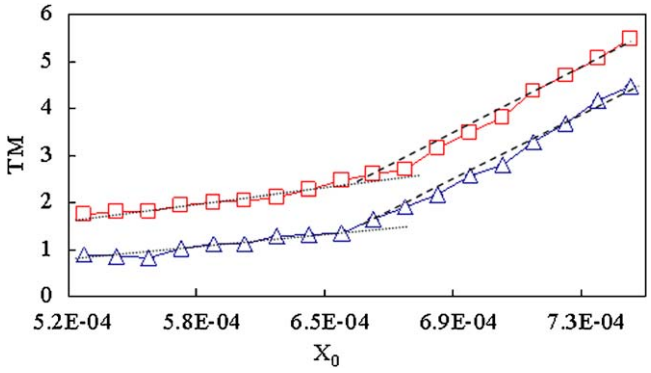

Fig. 8. Transmissibility TM as a function of the input displacement: $d = 2.6$ mm, $\eta = 0.57$, △—experiment, □—numerical simulation.

change in the degree of damping, particularly at 19 Hz as the input amplitude is changed. Therefore, subsequent investigations were focused on the system response as a function of the input displacement amplitude at the shifted resonance frequency of 19 Hz.

Figs. 9(a) and (b) illustrate the displacement trajectories of the masses and the velocity trajectory of the primary mass, respectively. For the numerical simulations, a 13 N driving force corresponding to the input amplitude of 0.57 mm was used. This input amplitude decreases in the lower TM region as seen in Fig. 7.

In Fig. 9(a), it is observed that regularly spaced dominant collisions occur when the primary mass passes the equilibrium position corresponding to the largest velocity of the primary mass and that the directions of movement of the masses are out-of-phase with (opposite to) each other. This out-of-phase motion affects the primary mass transferring momentum to the auxiliary mass with maximum kinetic energy loss. Fig. 9(b) shows an abrupt reduction in the value of the absolute velocity after each impact, which implies a loss of kinetic energy. This mechanism contributes to low values of TM and high damping in the left hand half of the input amplitude range shown in Fig. 6.

Different kinds of collisions are observed in Fig. 10 with an increased displacement input. In the numerical simulation results of the excitation force 18 N, seen in Figs. 10(a) and (b), it is observed that collisions occur when the velocity of the primary mass is near to zero, which results in less efficient momentum transfer.

The numerical simulation with an excitation force of 22 N, shown in Figs. 10(c) and (d), illustrates what happens with a larger magnitude displacement input. In particular, Fig. 10(c) demonstrates that the collisions take place with both masses travelling in the same direction. This kind of momentum transfer not only magnifies the amplitude of the primary mass but also adds the kinetic energy of the auxiliary mass to the primary mass without modifying the original system, resulting in a change in the resonance frequency of the system. It can thereby be inferred that the kinetic energy influx caused by impacts has a mass loading effect on the system. This description regarding the change of resonance frequency is different from the explanation provided by Masri and Ibrahim [16] and Duncan et al. [24] in their numerical study. They stated that the auxiliary mass sticks to the system so that two masses move together, when the system is operated with very large excitation amplitudes. Vibrations at resonance, however, if they are caused by in-phase impacts, do not require rigorous restrictions such as very large base amplitude inputs with $d \to \infty$ [16], $a' \to \infty$ [24], or stick motion. To this extent, the numerical simulation of the limiting case of the elastic impact ($e = 1$) emphasises the possibility that the mass loading effect, which causes a resonance shift can be explained without the assumption of stick motion, as shown in Fig. 11(a). Specifically, Fig. 11(b) establishes the fact that the auxiliary mass never sticks to the primary mass.

With respect to the numerical modelling of impacts, the analytical results of the proposed method are compared with those of the conventional method, as shown in Fig. 12. As can be seen, the simulation results of the proposed method are in better agreement with the experimental results than those of the conventional method, especially at the resonance frequency of 19 Hz. Moreover, the time trajectories of the analytical results demonstrate that there is a long period of grazing incidence before the auxiliary mass separates from the primary mass for the test condition of $N\mathrm{umr}_b$. Thus, the conventional method cannot represent resonance phenomena for the given condition, possibly due to the occurrence of repeated negative collisions.

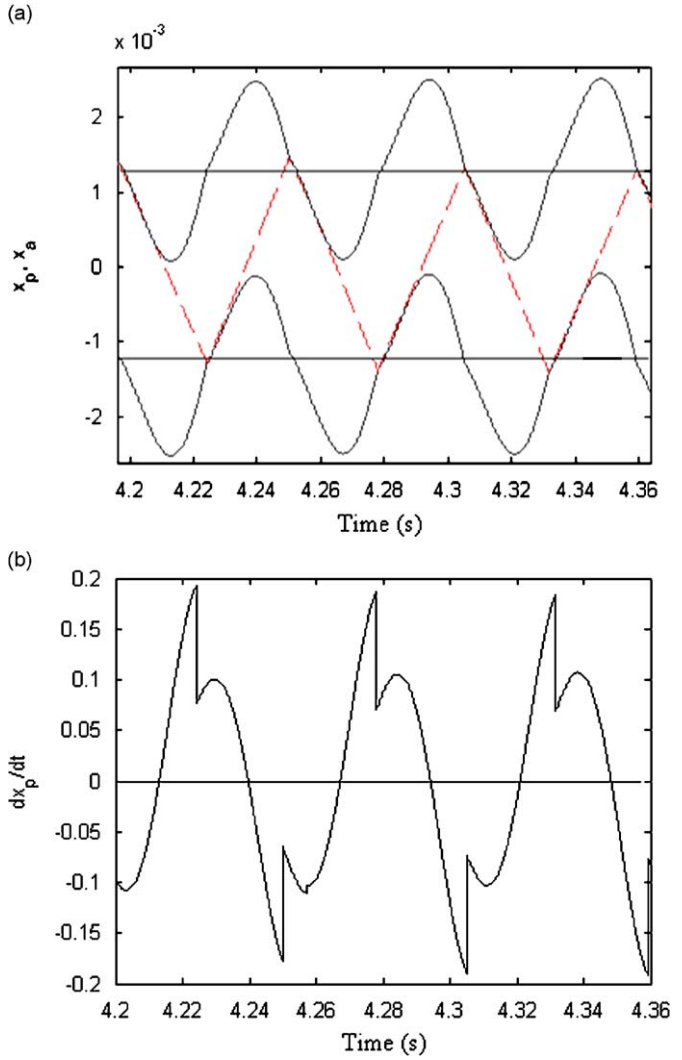

Fig. 9. Trajectories of the masses from numerical simulations at 19 Hz with 13 N driving force (d: 2.6 mm, η: 0.57): (a) displacement trajectories, dashed line-auxiliary mass, solid line-primary mass; (b) velocity trajectories of the primary mass.

The time trajectories of the numerical simulations provided significant insight into the resonance characteristics of the system. To validate the numerical simulation results, experimental results were considered.

Fig. 13 presents measured acceleration signals and the magnitude scaled velocity of the primary mass. Velocity histories were obtained by integrating the acceleration signal. Then, the magnitudes were scaled to show the times of the impacts. Measured acceleration signals are complicated because of the high frequency structural vibrations caused by the impacts. In Figs. 13(a)–(c), the abrupt acceleration peaks indicate impacts, and show good agreement with the numerical simulations given in Figs. 9 and 10.

With small magnitude displacement inputs where the damping is high, impacts occur at the maximum velocity of the primary mass, illustrated with arrows in Fig. 13(a), corresponding to the numerical simulations with 13 N in Fig. 9(a). Figs. 13(b) and (c), which correspond to the numerical simulations with input forces of 18 and 22 N, respectively, demonstrate how the time of impacts changes as the input amplitudes increase. The dashed circles in Fig. 13(c) indicate the times of impacts. It is observed that each impact takes places before the velocity of the primary mass reaches its maximum value, meaning that the auxiliary mass collides with the primary mass before its maximum stroke, which indicates unidirectional collisions are taking place.

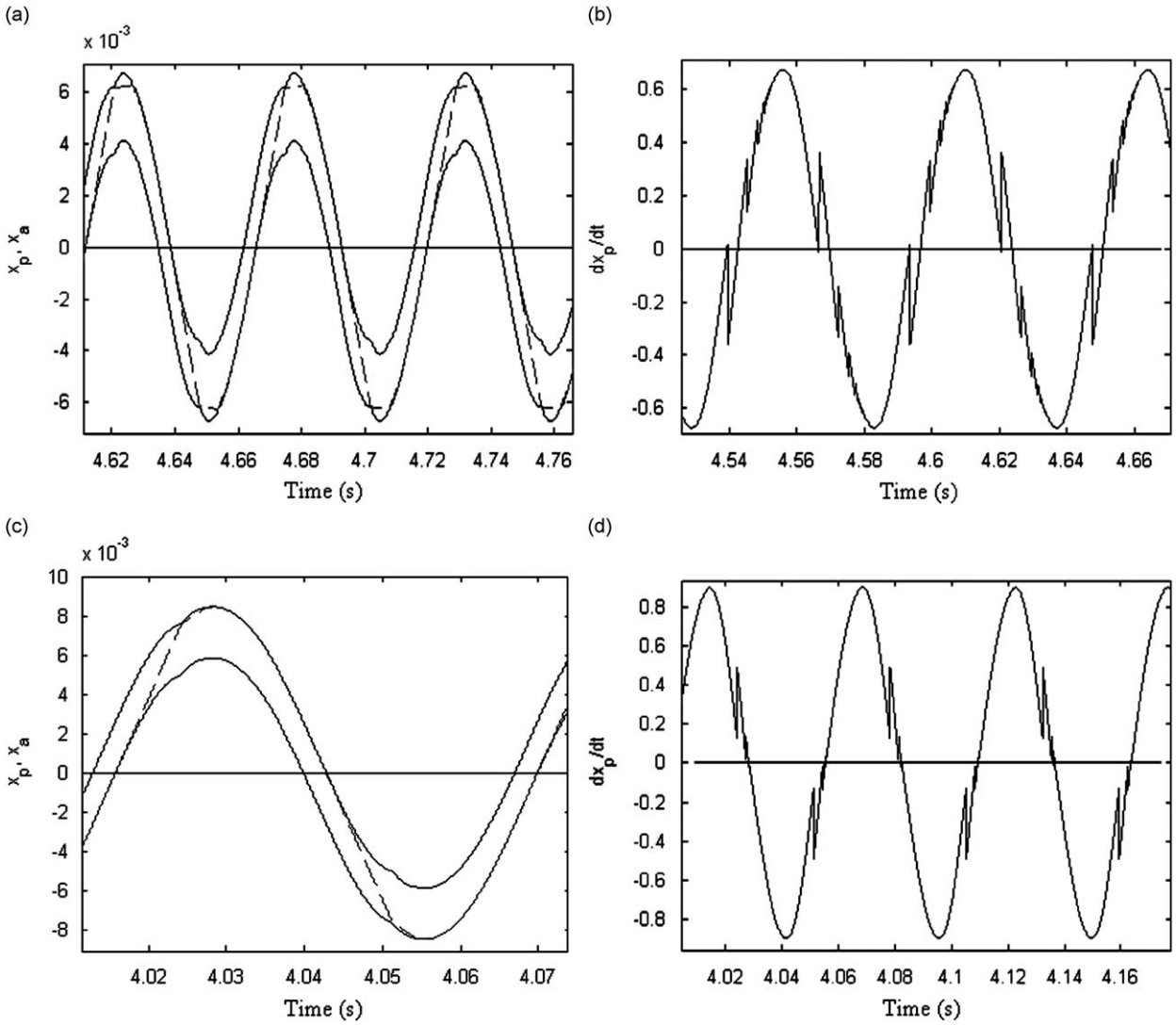

Fig. 10. Time trajectories of numerical simulations, dashed line-auxiliary mass; solid line-primary mass: (a) displacement trajectories ($F_0 = 18$ N); (b) velocity trajectory of the primary mass ($F_0 = 8$ N); (c) displacement trajectories ($F_0 = 22$ N); (d) velocity trajectory of the primary mass ($F_0 = 22$ N).

The experimental acceleration signals and scaled velocities corroborate the numerical simulation results and are in good agreement.

5. Discussion

It can be concluded from the experiments and numerical simulations that out-of-phase impacts reduce the displacement of the primary mass with efficient momentum transfer, or kinetic energy loss. Furthermore, the degree of damping depends on the type of the impact. In the limiting case, in-phase impacts occur, resulting in a mass loading effect caused by the flux of kinetic energy into the primary mass.

It has generally been accepted that it is important to achieve out-of phase motion to provide high efficiency of the impact damper [20], and that the magnitude of the displacement input and clearance are key factors, which determine whether the motion is in phase or out-of phase. Up to the present there has been little discussion about the resonance shift caused by impacts.

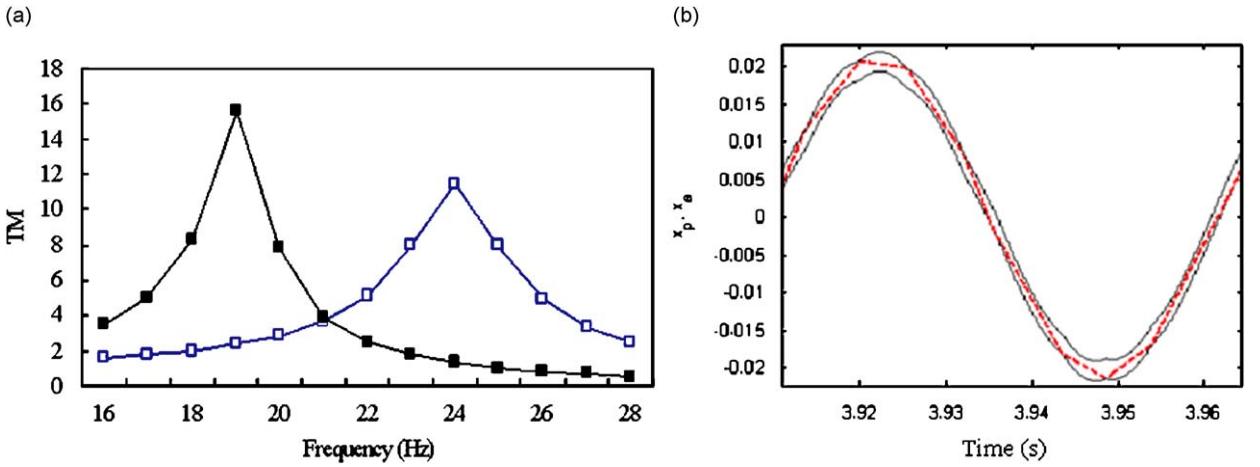

Fig. 11. Resonance shift with elastic collision ($e = 1$): (a) transmissibility, □—without auxiliary mass, ■—auxiliary mass installed, $X_{0\text{ref}} = 1.3$ mm; (b) Time trajectories, dotted line-auxiliary mass; solid line-primary mass.

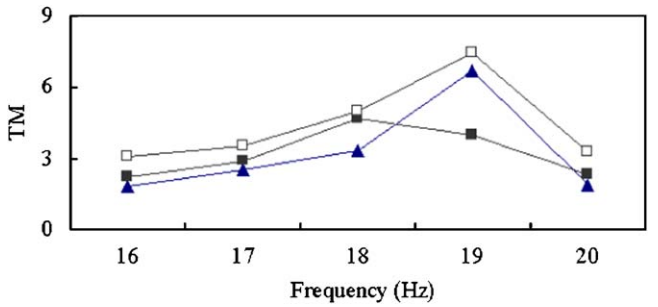

Fig. 12. Comparison of numerical methods governing contact and collision: ($e = 0.2$, $\eta = 0.57$, Exp_b and Numr_b in Table 2), ▲—experiment, ■—conventional method, □—proposed method.

In the past, the magnitude of the momentum transfer was used to predict the efficiency of the impact damper as a function of the input amplitude [24]. Eq. (11) represents the mass normalized relative momentum transfer.

$$\Lambda = \frac{(\dot{X}_p^+ - \dot{X}_p^-)}{\dot{X}_{\text{pabs}}}, \tag{11}$$

where Λ is the mass normalized relative momentum transfer, and $\dot{X}_{\text{pabs}}$ is the Fourier transformed velocity of the primary mass.

However, the kinetic energy transfer and the direction of transfer have different characteristics from the impact damper. The normalized kinetic energy transfer can be written as

$$\Phi = \frac{(|\dot{X}_p^+| - |\dot{X}_p^-|)}{\dot{X}_{\text{pabs}}}, \tag{12}$$

where Φ is the normalized kinetic energy transfer.

Figs. 14(a) and (b) represent the mass normalized relative momentum transfer and the normalized kinetic energy transfer as functions of the input force, respectively. Fig. 14(a) further illustrates the decrease in damping efficiency, which occurs with increasing input amplitudes. This result is consistent with previous investigations [24]. However, different characteristics of the impact damper are observed in Fig. 14(b), which suggests that the kinetic energy transfer switches the direction of transfer just after the input force becomes larger than 18 N. In Figs. 14(a) and (b), the shift in resonance vibration corresponding to a 22 N input force is

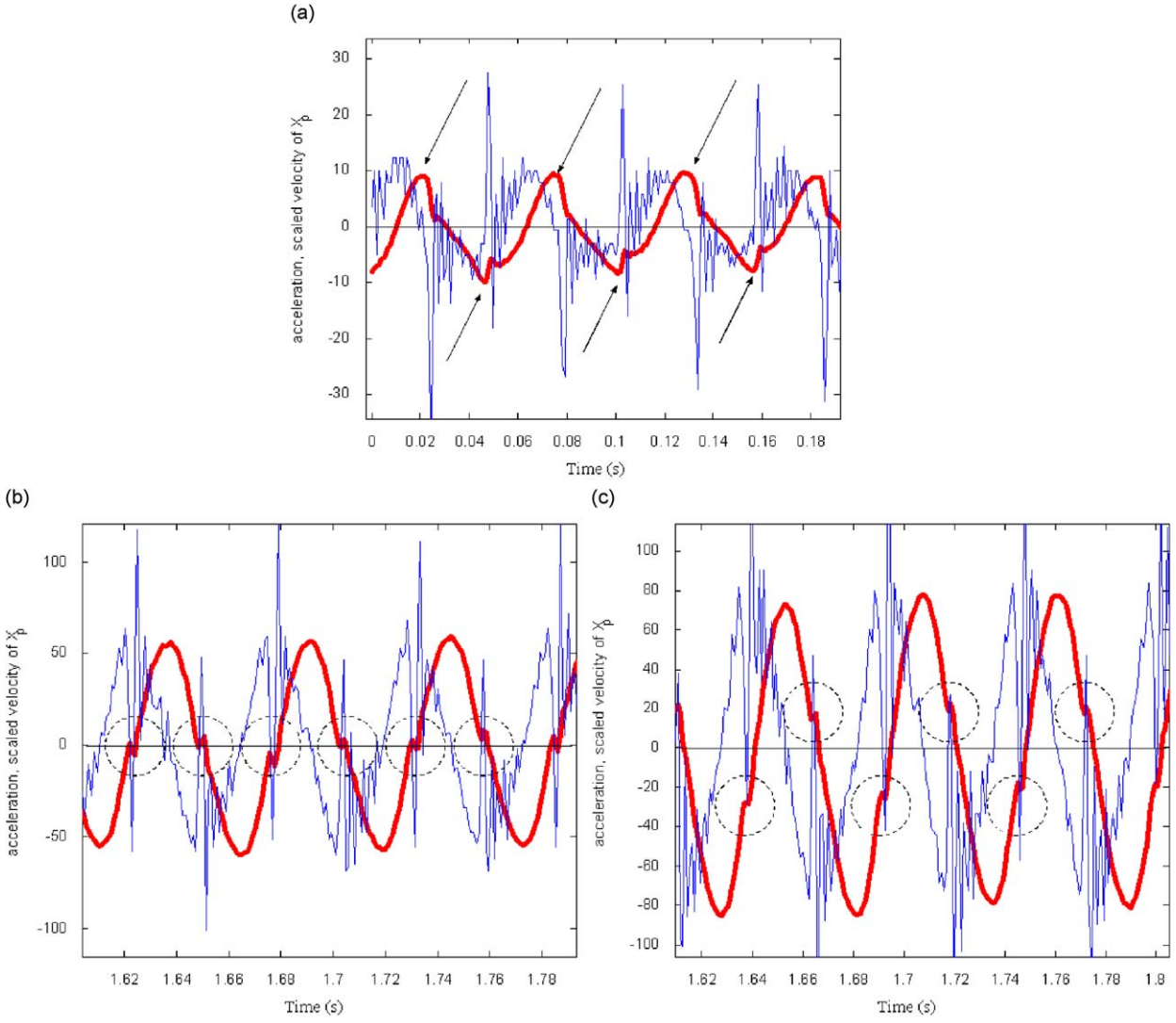

Fig. 13. Experimental acceleration and scaled velocity at 19 Hz, arrows indicate the times of impact in (a), dashed circles enclose the time of impact in (b) and (c): ▬ magnitude scaled velocity, — acceleration, (a) 0.53 mm input displacement corresponding to $F_0 = 12$ N, (b) 0.75 mm input displacement corresponding to $F_0 = 18$ N, (c) 0.97 mm input displacement corresponding to $F_0 = 22$ N.

circled. A quantitative analysis of momentum transfer presents a good description for the decrease in the degree of damping as a function of the input force. But, it cannot represent mass loading caused by impacts. However, the qualitative analysis of the kinetic energy as a function of input force, presented experimentally and numerically in this paper, gives specific information about the mass loading effect and shift in resonance vibrations.

A previous study [23] presented a frequency criterion for negative damping implicitly, as given in Eq. (13).

$$r < (1+\eta)^{-1/2}, \tag{13}$$

where r is the frequency ratio of driving frequency to natural frequency, and η is the mass ratio.

Our research is concerned with the resonance frequency of the impact damper. In order to predict the shift in the resonance frequency, *Rayleigh's energy method*, Eq. (14), for a system undergoing simple harmonic motion is considered.

$$T_{\max} = \tfrac{1}{2} m \dot{X}^2_{\max} = \tfrac{1}{2} k X^2_{\max} = U_{\max}, \tag{14}$$

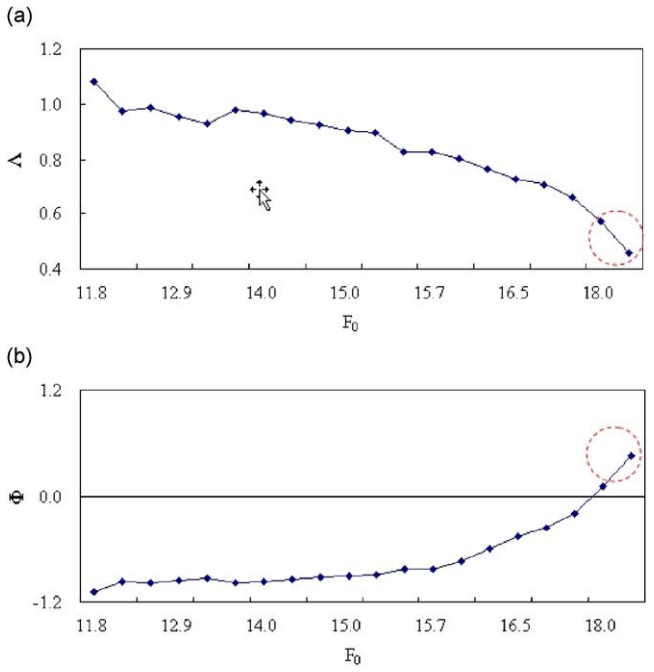

Fig. 14. Mass normalized relative momentum transfer and normalized kinetic energy transfer: (a) mass normalized relative momentum transfer; (b) normalized kinetic energy transfer.

where T and U refer to the kinetic energy and potential energy of the system, respectively, and the subscript "max" represents the maximum value.

Fig. 15 illustrates velocities of the primary and auxiliary mass. The absolute values of the maximum velocities of the primary and auxiliary masses can be regarded as the same when in-phase impacts dominate except the time duration in which the auxiliary mass is separated from the primary mass and moves alone represented with dashed line in Fig. 15. Fig. 15(b) shows trajectories of the system at the time of separation and impacts. After separated from the primary mass, the auxiliary mass maintains its velocity before it collides with the primary mass. Consequently, the maximum displacement of the system is affected by the kinetic energy influx during the impact.

For the system under consideration, Eq. (14) becomes Eq. (15) on the condition that in-phase impacts dominate the dynamics of the system.

$$T_{\max} = \tfrac{1}{2}(m_p + m_a)\dot{\chi}^2_{\max} = \tfrac{1}{2}k\chi^2_{\max} = U_{\max}, \tag{15}$$

where χ is displacement of the primary mass resulting from the kinetic energy influx.

The resulting resonance frequency of the system undergoing kinetic energy influx caused by the impacts can then be written as

$$\omega_{\text{in}} = \sqrt{\frac{k}{m_p + m_a}}, \tag{16}$$

where ω_{in} is the shifted resonance frequency of the impact damper.

Subsequently, the shift in resonance frequency was investigated experimentally as a function of the mass ratio, and the displacement ratio, ψ, the ratio of displacement of the primary mass to the clearance. In previous studies, the displacement ratio was an empirical criterion used in both experimental and numerical investigations [17,19,20,23]. It was assumed that the criterion should not exceed unity in order to stabilize the damping effect of the impact damper without mentioning the specific frequency. This criterion was employed to avoid the ambiguous description of the condition, "large amplitude" to describe the decrease in damping with large amplitude excitation.

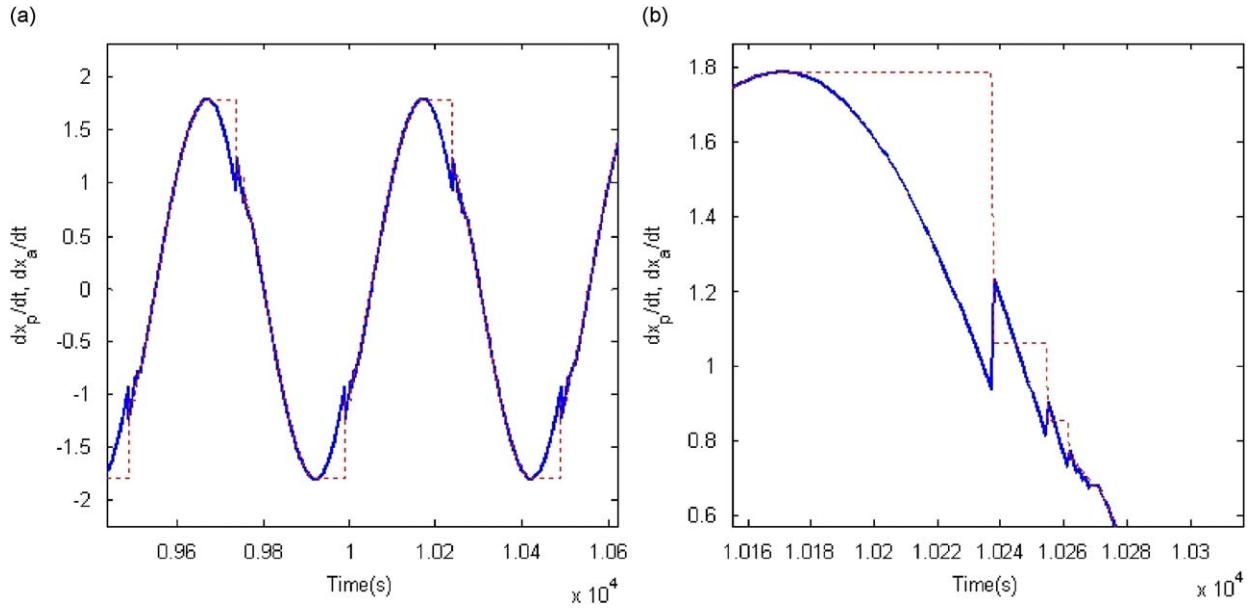

Fig. 15. Velocity of the primary mass and the auxiliary mass: solid line-primary mass; dashed line-auxiliary mass: (a) trajectories; (b) time of separation and impacts.

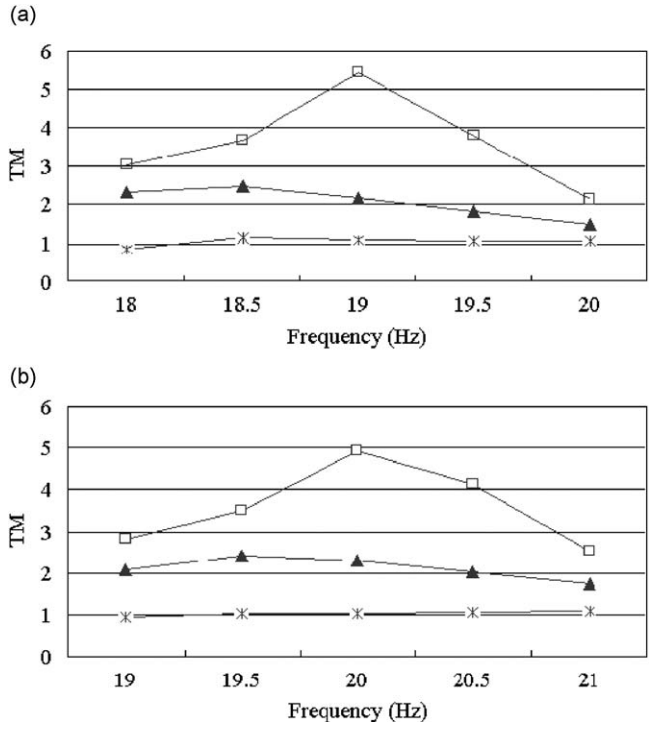

Fig. 16. Frequency responses of the experimental results as a function of the mass ratio: (a) $\eta = 0.57$, $d = 2.6$ mm, □—$\psi = 2.7$; ▲—$\psi = 1.9$; ✻—$\psi = 0.5$, (b) $\eta = 0.4$, $d = 4$ mm, □—$\psi = 1.9$; △—$\psi = 1.1$; ✻—$\psi = 0.5$.

Fig. 16 illustrates the correlation of the mass ratio and resonance frequency shift with respect to the displacement ratio. The expected values of the shifted resonances based on Eq. (16) are 19 and 20 Hz for mass ratios of 0.57 and 0.4, respectively.

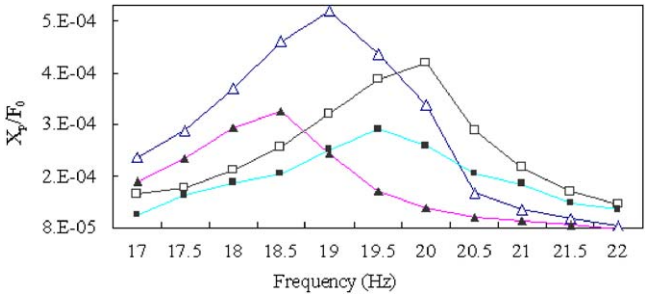

Fig. 17. Frequency responses of the numerical simulations as a function of the mass ratio and phase of the impact: (□—$\eta = 0.4$, △—$\eta = 0.57$), in-phase impact; (■—$\eta = 0.4$, ▲—$\eta = 0.57$), before in-phase impact.

The results presented in Fig. 16 show that the resonance shifts are predictable when the mass loading effect of the auxiliary mass is considered. Also, it is observed that the displacement ratio can be used as a general guideline for the system performance. Moreover, acceleration signals of curves of $\psi = 2.7$ in Fig. 16(a), and $\psi = 1.9$ in Fig. 16(b), are seen to be for in-phase impacts.

Fig. 17 illustrates the dependence of the resonance shift on the mass ratio in a numerical simulation. If the vibration amplitude of the primary and auxiliary masses satisfies the in-phase impact condition, then the resonance frequency is a function of the mass ratio. The analytical results in Fig. 17 show exactly the same frequency shifts as the experimental results presented in Figs. 16(a) and (b).

The implication of these experimental results and numerical simulations is that a freely moving mass undergoing periodic impacts can have a mass loading effect on a system, resulting in a shift in resonance frequency, which is related to the phase of the impacts. In addition, the resonance frequency shift caused by an in-phase impact has a different effect on the system and depends on the mass ratio and forcing frequency.

Some investigators have presented mass loading effects in their numerical studies of impact dampers with the postulation that the displacement of the primary system is large enough so that $d \to \infty$ and $a' \to \infty$. These conditions make the auxiliary mass stick to the primary mass [16,24]. However, our experiments show that with practical vibration levels, the auxiliary mass can have a mass loading effect causing a shift in resonance frequency which should be avoided in order to ensure system stability.

It is noted that the transition from kinetic energy loss to kinetic energy influx caused by impacts and their relationship to the increase in excitation amplitude is a general phenomenon, which is independent of the forcing frequency. It is an inherent characteristic of a system undergoing impacts with a fixed clearance. The consequences of the mass loading by impacts caused by large amplitude excitation depend on the frequency and mass ratios. Thus, the resonance phenomenon should be considered in the design of an impact damper to ensure the stability of the system.

6. Conclusions

Dynamic responses of impact dampers have been investigated experimentally and numerically with a primary focus on the vibrations at resonance. An improved scheme for detecting the time of impact has been developed in order to prevent negative collisions, which represent an intolerable scenario for large amplitude vibrations. Detailed experiments with a horizontal impact damper explain the general performance and the resonance vibration of the integrated system, which occurs at a frequency, which is different from the original resonance frequency.

Furthermore, numerical simulations of mass trajectories demonstrate how the relative motion of the masses is related to the degree of damping. It was found that an out-of-phase impact produces the most effective damping, and that the efficiency of the momentum transfer decreases with an increase in input amplitudes. These conditions agree with previous studies. However, it is observed from the experiments and numerical simulations that an in-phase impact between the primary and auxiliary masses induces kinetic energy influx into the primary system, resulting in a mass loading effect and a shift in resonance frequency.

Thus a simple model for the prediction of mass loading effects has been formulated, which is based on observations. Simulations show that the numerical predictions are in good agreement with experimental observations.

References

[1] M.J. Crocker (Ed.), *Handbook of Noise and Vibration Control*, Wiley, New York, 2007 (Chapters 15, 59–62 and 64).
[2] L. Gelman, P. Jenkins, I. Petrunini, M.J. Crocker, Vibroacoustical damping diagnostics: complex frequency response function versus its magnitude, *International Journal of Acoustics and Vibration* 11 (2006) 120–124.
[3] L. Xu, X. Jia, Electromechanical coupled vibration for double coupled micro beams, *International Journal of Acoustics and Vibration* 12 (2007) 24–51.
[4] H.K. Hornig, G.T. Flowers, Performance of heuristic optimisation methods in the characterisation of the dynamic properties of sandwich composite materials, *International Journal of Acoustics and Vibration* 12 (2007) 60–68.
[5] A.S. Simon, G.T. Flowers, Adaptive disturbance rejection and stabilisation for rotor systems with internal damping, *International Journal of Acoustics and Vibration* 13 (2008) 73–81.
[6] K.M.J. Tammi, Identification and active feedback–feedforward control of rotor, *International Journal of Acoustics and Vibration* 12 (2007) 7–14.
[7] H. Akesson, T. Smirnova, I. Claesson, L. Hakkansson, On the development of a simple and robust active control system for boring bar vibration in industry, *International Journal of Acoustics and Vibration* 12 (2007) 139–152.
[8] L. Chen, C.H. Hansen, F. He, K. Summut, Active nonlinear vibration absorber design for flexible structures, *International Journal of Acoustics and Vibration* 12 (2007) 51–59.
[9] R.D. Friend, V.K. Kinra, Particle impact damping, *Journal of Sound and Vibration* 233 (2000) 93–118.
[10] S.E. Olson, An analytical particle damping model, *Journal of Sound and Vibration* 264 (2003) 1155–1166.
[11] Z. Xu, M.Y. Wang, T. Chen, Particle damping for passive vibration suppression: numerical modeling and experimental investigation, *Journal of Sound and Vibration* 279 (2005) 1097–1120.
[12] A.L. Paget, Vibration in steam turbine buckets and damping by impacts, *Engineering* 143 (1937) 305–307.
[13] C. Grubin, On the theory of acceleration damper, *Journal of Applied Mechanics, Transactions of the ASME* 78 (1956) 373–378.
[14] S.F. Masri, T.K. Caughey, On the stability of the impact damper, *Journal of Applied Mechanics, Transactions of the ASME* 33 (1966) 586–592.
[15] S.F. Masri, General motion of impact damper, *Journal of the Acoustical Society of America* 47 (1970) 229–237.
[16] S.F. Masri, A.M. Ibrahim, Response of the impact damper to stationary random excitation, *Journal of the Acoustical Society of America* 53 (1973) 200–211.
[17] N. Popplewell, C.N. Bapat, K. McLachlan, Stable periodic vibroimpacts of an oscillator, *Journal of Sound and Vibration* 87 (1983) 41–59.
[18] L.A. Chen, S.E. Semercigil, A beam-like damper for attenuating transient vibrations of light structures, *Journal of Sound and Vibration* 164 (1993) 53–65.
[19] S. Ema, E. Marui, A fundamental study on impact dampers, *International Journal of Machine Tools & Manufacture* 34 (1994) 407–421.
[20] C.C. Cheng, J.Y. Wang, Free vibration analysis of a resilient impact damper, *International Journal of Mechanical Sciences* 45 (2003) 589–604.
[21] S. Chatterjee, A.K. Mallik, Bifurcations and chaos in autonomous self-excited oscillators with impact damping, *Journal of Sound and Vibration* 191 (1996) 539–562.
[22] G. Luo, L. Ma, X. Lv, Dynamic analysis and suppressing chaotic impacts of a two-degree-of-freedom oscillator with a clearance, *Nonlinear Analysis: Real World Applications* 10 (2009) 756–778.
[23] C.N. Bapat, S. Sankar, Single unit impact damper in free and forced vibration, *Journal of Sound and Vibration* 99 (1985) 85–94.
[24] M.R. Duncan, C.R. Wassgren, C.M. Krousgrill, The damping performance of a single particle impact damper, *Journal of Sound and Vibration* 286 (2005) 123–144.
[25] S. Ekwaro-Osire, C. Ozerdim, M.P.H. Khandaker, Effect of attachment configuration on impact vibration absorbers, *Experimental Mechanics* 46 (2006) 669–681.
[26] A.M. Rahman, C.A. Edwards, Electricity: taxes on emission liabilities. An examination of the economic effectiveness of Polluter Pays Principles, *Energy Policy* 32 (2004) 221–235.
[27] E. Delarue, H. Lamberts, W. D'haeseleer, Simulating greenhouse gas (GHG) allowance cost and GHG emission reduction in Western Europe, *Energy* 32 (2007) 1299–1309.
[28] H. Tsuchiya, WWF Scenario for Solving the Global Warming Problem Index for 2010 and 2020, p. 11.
[29] Y. Beck, B. Bishara,, D. Medini, Connecting an alternative energy source to the power grid by a DSP controlled DC/AC inverter, *2005 Proceedings of the Inaugural IEEE PES 2005 Conference and Exposition in Africa 2005*, art. no. 1611798, pp. 120–124.
[30] S.M. Jeter, W.J. Wepfer, G.M. Fadel, N.E. Cowden, A.A. Dymek, Variable speed drive heat pump performance, *Energy* 12 (1987) 1289–1298.
[31] C. Aprea, R. Mastrullo, C. Renno, Experimental analysis of the scroll compressor performances varying its speed, *Applied Thermal Engineering* 26 (2006) 983–992.

[32] Y.P. Zhou, J.Y. Wu, R.Z. Wang, S. Shiochi, Energy simulation in the variable refrigerant flow air-conditioning system under cooling conditions, *Energy and Buildings* 39 (2007) 212–220.
[33] H. Li, S.-K. Jeong, J.-I. Yoon, S.-S. You, An empirical model for independent control of variable speed refrigeration system, *Applied Thermal Engineering* 28 (2008) 1918–1924.
[35] S.E. Semercigil, F. Collette, D. Huynh, Experiments with tuned absorber—impact damper combination, *Journal of Sound and Vibration* 256 (2002) 179–188.
[36] K. Li, A.P. Darby, An experimental investigation into the use of a buffered impact damper, *Journal of Sound and Vibration* 291 (2006) 844–860.
[37] S. Ma, S.E. Semercigil, A modified passive tuned absorber for secondary systems under random excitation, *Journal of Sound and Vibration* 208 (1997) 349–366.
[38] V.G. Ivancevic, T.T. Ivancevic, Complex nonlinearity: combining it all together, *Understanding Complex Systems* (2008) 657–711.
[39] L.A. Bergman, M. Shinozuka, C.G. Bucher, K. Sobczyk, G. Dasgupta, P.D. Spanos, G. Deodatis, R. Zhang, A state-of-the-art report on computational stochastic mechanics, *Probabilistic Engineering Mechanics* 12 (1997) 197–321.
[40] M.H. Fredriksson, Grazing bifurcations in multibody systems, *Nonlinear Analysis, Theory, Methods & Applications* 30 (1997) 4475–4483.
[41] H. Dankowicz, X. Zhao, Local analysis of co-dimension-one and co-dimension-two grazing bifurcations in impact microactuators, *Physica D* 202 (2005) 238–257.
[42] A. Jimeno, S. Cuenca, Reconfigurable computing for tool-path computation, *The International Journal of Advanced Manufacturing Technology* 21 (2003) 945–951.